

Guiding and confining light in void nanostructure

Vilson R. Almeida, Qianfan Xu, Carlos A. Barrios, and Michal Lipson

School of Electrical and Computer Engineering, Cornell University, 411 Phillips Hall, Ithaca, New York 14853

Received January 20, 2004

We present a novel waveguide geometry for enhancing and confining light in a nanometer-wide low-index material. Light enhancement and confinement is caused by large discontinuity of the electric field at high-index-contrast interfaces. We show that by use of such a structure the field can be confined in a 50-nm-wide low-index region with a normalized intensity of $20 \mu\text{m}^{-2}$. This intensity is approximately 20 times higher than what can be achieved in SiO_2 with conventional rectangular waveguides. © 2004 Optical Society of America

OCIS codes: 030.4070, 130.0130, 130.2790, 230.7370, 230.7380, 230.7390, 230.7400.

Recent results in integrated optics have shown the ability to guide, bend, split, and filter light on chips by use of optical devices based on high-index-contrast waveguides.^{1–5} In all these devices the guiding mechanism is based on total internal reflection (TIR) in a high-

being formed by the interaction between the fundamental eigenmodes of the individual slab waveguides. Rigorously, the analytical solution for the transverse E-field profile E_x of the fundamental TM eigenmode of the slab-based slot waveguide is

$$E_x(x) = A \begin{cases} \frac{1}{n_S^2} \cosh(\gamma_S x), & |x| < a \\ \frac{1}{n_H^2} \cosh(\gamma_S a) \cos[\kappa_H(|x| - a)] + \frac{\gamma_S}{n_S^2 \kappa_H} \sinh[\kappa(|x| - a)], & a < |x| < b \\ \frac{1}{n_C^2} \left\{ \cosh(\gamma_S a) \cos[\kappa_H(b - a)] + \frac{n_H^2 \gamma_S}{n_S^2 \kappa_H} \sinh(\gamma_S a) \sin[\kappa_H(b - a)] \right\} \exp[-\gamma_C(|x| - b)], & |x| > b \end{cases} \quad (1)$$

index material (core) surrounded by a low-index material (cladding); the TIR mechanism can strongly confine light in the high-index material. In recent years a number of structures have been proposed to guide or enhance light in low-index materials,^{6–11} relying on external reflections provided by interference effects. Unlike TIR, the external reflection cannot be perfectly unity; therefore the modes in these structures are inherently leaky modes. In addition, since interference is involved, these structures are strongly wavelength dependent.

Here we show that the optical field can be enhanced and confined in the low-index material even when light is guided by TIR. For a high-index-contrast interface, Maxwell's equations state that, to satisfy the continuity of the normal component of electric flux density D , the corresponding electric field (E-field) must undergo a large discontinuity with much higher amplitude in the low-index side. We show that this discontinuity can be used to strongly enhance and confine light in a nanometer-wide region of low-index material. The proposed structure presents an eigenmode, and it is compatible with highly integrated photonics technology.

The principle of operation of the novel structure can be illustrated by analysis of the slab-based structure shown in Fig. 1(a), where a low-index slot is embedded between two high-index slabs (shaded regions). The novel structure is hereafter referred to as a slot waveguide. The slot waveguide eigenmode can be seen as

where κ_H is the transverse wave number in the high-index slabs, γ_C is the field decay coefficient in the cladding, γ_S is the field decay coefficient in the slot, and constant A is given by

$$A = A_0 \frac{\sqrt{k_0^2 n_H^2 - \kappa_H^2}}{k_0}, \quad (2)$$

where A_0 is an arbitrary constant and $k_0 = 2\pi/\lambda_0$ is the vacuum wave number. The transverse parameters κ_H , γ_S , and γ_C simultaneously obey the relations $k_0^2 n_H^2 - \kappa_H^2 = k_0^2 n_C^2 + \gamma_C^2 = k_0^2 n_S^2 + \gamma_S^2 = \beta^2$, where β is the eigenmode propagation constant, which can be calculated by solving the transcendental characteristic equation

$$\tan[\kappa_H(b - a) - \Phi] = \frac{\gamma_S n_H^2}{\kappa_H n_S^2} \tanh(\gamma_S a), \quad (3)$$

where $\Phi = \arctan[\gamma_C n_H^2 / (\kappa_H n_C^2)]$.

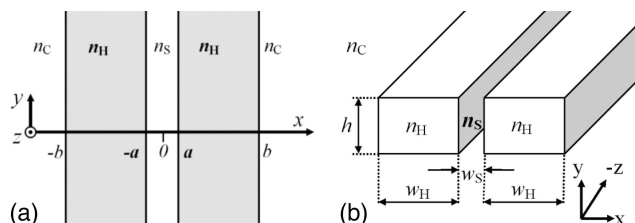


Fig. 1. Schematic of the slot waveguide structure (a) with infinite height and (b) with finite height.

From Eq. (1) the E-field immediately inside the slot ($|x| = a^-$) is n_H^2/n_S^2 times higher than that immediately inside the high-index slabs ($|x| = a^+$). The ratio n_H^2/n_S^2 equals 6 for a Si-SiO₂ interface and 12 for a Si-air interface. When the width of the slot is much smaller than the characteristic decay length inside the slot ($a \ll 1/\gamma_S$), the field remains high all across the slot. By assuming that $n_H = 3.48$, $n_S = n_C = 1.44$, $a = 25$ nm, and $b = 205$ nm, we calculated the TM E_x distribution at $\lambda_0 = 1.55$ μm . Figure 2 shows that the E_x distribution, which evidences the large discontinuity and the high E-field confinement in the slot; in this case $a = 25$ nm $\ll 1/\gamma_S = 140$ nm.

Hereafter we consider a three-dimensional (3D) slot waveguide structure with finite height [see Fig. 1(b)]. In this case the quasi-TE eigenmode presents the major E-field component along the x direction. Therefore the quasi-TE eigenmode in the 3D slot waveguide structure is analogous to the TM eigenmode in the studied slab-based slot waveguide structure. We calculated the quasi-TE eigenmode of the 3D slot waveguide structure with a nonuniform grid mesh full-vectorial finite-difference mode solver, taking material dispersion into account.¹² We assume that the slot waveguide is built on a silicon-on-insulator (SOI) platform; therefore $n_H = 3.48$, $n_C = 1.44$, and $\lambda_0 = 1.55$ μm are assumed, unless otherwise specified. We also assume that the rectangular cross-section slot, with height h and width w_S , is filled with SiO₂ ($n_S = 1.44$); in practice, the slot can be filled with any low-index material of interest.

The transverse E-field distribution of the quasi-TE mode is shown in Fig. 3. We assume $w_H = 180$ nm, $w_S = 50$ nm, and $h = 300$ nm, unless otherwise specified. Figure 3(a) shows the contours of the E-field amplitude and the E-field lines. The center bright region shows a strong E-field inside the slot. The directions of the E-field lines in the slot confirm that the E-field is mostly normal to the high-index-contrast interface, which induces its strong discontinuity. The amplitude profile of the E-field is shown in the 3D surface plot shown in Fig. 3(b). One can see that the amplitude profile of the E-field along the x direction at $y = 0$ strongly resembles that in Fig. 2 for the slab-based counterpart. The vertical confinement of the E-field in the slot region is dictated by that in the high-index regions. Since the slot waveguide structure has a true eigenmode, it is theoretically lossless.

As a result of the E-field enhancement in the slot, the optical intensity there is also much higher than that in the high-index regions. Figure 4 shows optical power P_{slot} and average optical intensity $I_{\text{slot}} = P_{\text{slot}}/(hw_S)$ inside the slot as a function of its width w_S and width of the silicon region w_H . Both P_{slot} and I_{slot} are normalized with respect to the total waveguide optical power. For comparison, the normalized average intensity in the silicon region I_{Si} is plotted as well. Figure 4 shows that P_{slot} remains nearly constant around 30% for $w_S \geq 50$ nm. For $w_S = 50$ nm, I_{slot} is as high as $20 \mu\text{m}^{-2}$, which is 6 times higher than I_{Si} . One can also see from Fig. 4 that w_H does not significantly affect the slot waveguide performance.

Light propagation in the slot waveguide shows a much higher intensity than that achievable with conventional waveguides. The highest normalized average intensity in a conventional SOI waveguide is less than $9 \mu\text{m}^{-2}$ for an optimal cross section of $360 \text{ nm} \times 200 \text{ nm}$. For SiO₂-air platform, this parameter reduces to less than $1.1 \mu\text{m}^{-2}$ for an optimal cross section of $900 \text{ nm} \times 500 \text{ nm}$; this is approximately 20 times lower than that of the presented slot

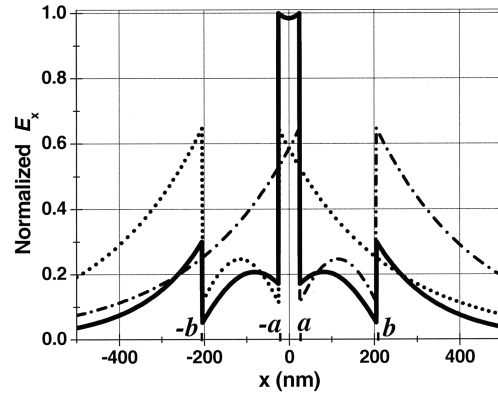


Fig. 2. Normalized transverse E-field (E_x) distribution of the fundamental TM eigenmode (solid curve) for the slab-based slot waveguide at $\lambda_0 = 1.55$ μm , with $n_H = 3.48$, $n_S = n_C = 1.44$, $a = 25$ nm, and $b = 205$ nm. Also shown are the individual slab waveguide TM eigenmodes (dotted and dashed-dotted curves).

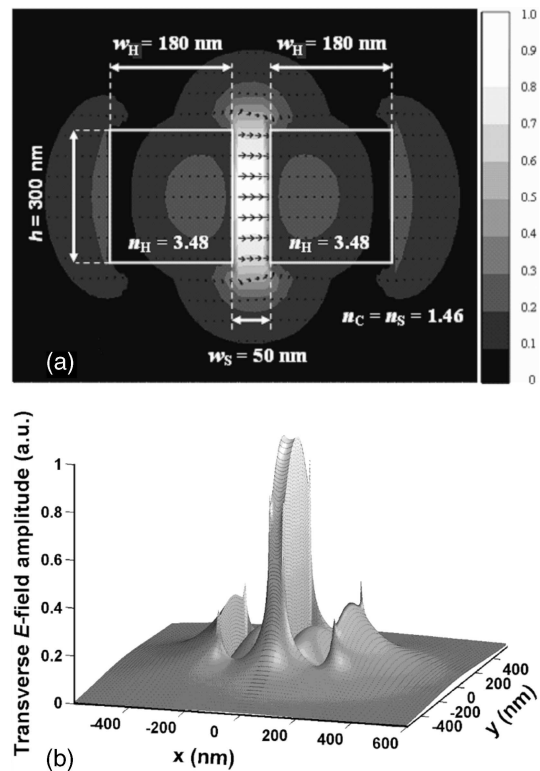


Fig. 3. Transverse E-field profile of the quasi-TE mode in a SOI-based slot waveguide. The origin of the coordinate system is located at the center of the waveguide, with a horizontal x axis and a vertical y axis. (a) Contour of the E-field amplitude and the E-field lines. (b) 3D surface plot of the E-field amplitude.

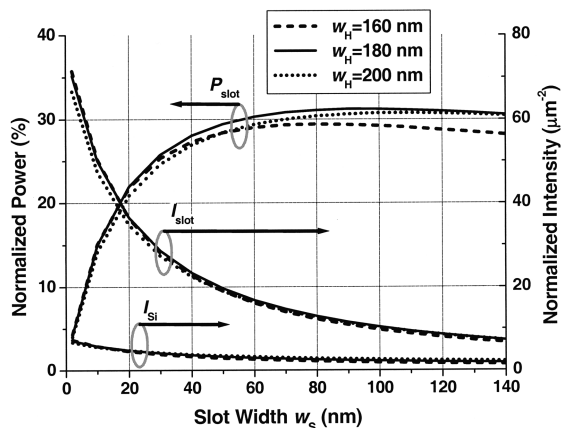


Fig. 4. Normalized optical power in slot P_{slot} , normalized average optical intensity in slot I_{slot} , and normalized average optical intensity in silicon I_{Si} , for the fundamental quasi-TE eigenmode of the slot waveguide. All quantities are normalized with respect to the waveguide optical power.

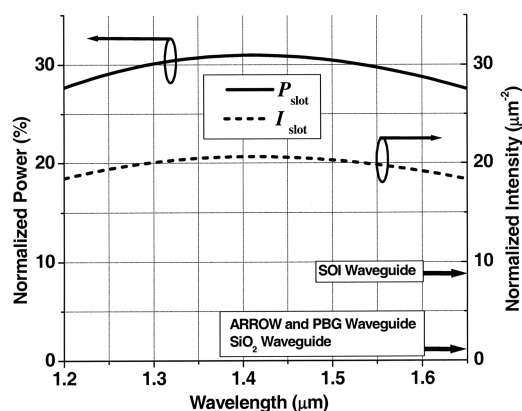


Fig. 5. Wavelength dependence of normalized optical power P_{slot} and normalized average optical intensity I_{slot} in the slot, for $w_H = 180$ nm, $w_s = 50$ nm, and $h = 300$ nm. Optimal values for the normalized optical intensity of alternative waveguide approaches are also indicated. ARROW, antiresonant reflecting optical waveguide; PBG, photonic bandgap.

waveguide. For leaky-mode waveguides based on external reflections, such as antiresonant reflecting optical waveguides and photonic crystal waveguides, the size of the low-index core is limited to being larger than half of the wavelength in the low-index material. Therefore the normalized intensity can hardly exceed $1 \mu\text{m}^{-2}$ at a wavelength of $\lambda_0 = 1.55 \mu\text{m}$.

We simulated P_{slot} and I_{slot} wavelength dependence (see Fig. 5). The structure presents very low wavelength sensitivity because there is no interference effect involved in the guiding and confinement mechanism. One can see that P_{slot} and I_{slot} vary less than 10% over a wavelength span of more than 400 nm. As a comparison, Fig. 5 shows the optical intensity levels for the alternative approaches discussed in the previous paragraph.

We verified the slot waveguide compatibility with highly integrated photonics technology. For a bending radius of only $R = 5 \mu\text{m}$ the transmission in a

360° turn is 99.2%, implying bending loss of 11 dB/cm. This result is particularly relevant for the fabrication of high-quality ring resonators, where such bending losses translate into a quality factor of $Q = 20,000$.

In summary, we have presented a novel waveguide geometry for guiding and confining light in a low-index region. The waveguide discussed has two unique properties. First, it produces high E-field amplitude, optical power, and optical intensity in low-index materials at levels that cannot be achieved with conventional waveguides. This property allows highly efficient interaction between fields and active materials, which may lead to all-optical switching and parametric amplification on integrated photonics. Second, a strong E-field confinement is localized to a nanometer-sized low-index region; therefore the slot waveguide can be used to greatly increase the sensitivity of compact optical sensing devices or to enhance the efficiency of near-field optical probes.

The authors thank Christina Manolatu for her guidance and assistance in the simulations and Roberto R. Panepucci for fruitful discussions. This work was supported by the Air Force Office of Scientific Research under grant AFOSR F49620-03-1-0424. V. R. Almeida acknowledges sponsorship support provided by the Brazilian Defense Ministry. M. Lipson's e-mail address is lipson@ece.cornell.edu.

References

1. K. K. Lee, D. R. Lim, L. C. Kimerling, J. Shin, and F. Cerrina, *Opt. Lett.* **26**, 1888 (2001).
2. A. Sakai, G. Hara, and T. Baba, *Proc. SPIE* **4283**, 610 (2001).
3. C. Manolatu, S. G. Johnson, S. Fan, P. R. Villeneuve, H. A. Haus, and J. D. Joannopoulos, *J. Lightwave Technol.* **17**, 1682 (1999).
4. R. L. Espinola, R. U. Ahmad, F. Pizzuto, M. J. Steel, and R. M. Osgood, *Opt. Express* **8**, 517 (2001), <http://www.opticsexpress.org>.
5. B. E. Little, J. S. Foresi, G. Steinmeyer, E. R. Thoen, S. T. Chu, H. A. Haus, E. P. Ippen, L. C. Kimerling, and W. Greene, *IEEE Photon. Technol. Lett.* **10**, 549 (1998).
6. M. A. Duguay, Y. Kokubun, and T. L. Koch, *Appl. Phys. Lett.* **49**, 13 (1986).
7. R. Bernini, S. Campopiano, L. Zeni, C. de Boer, and P. M. Sarro, in *Proceedings of IEEE First International Conference on Sensors* (Institute of Electrical and Electronics Engineers, New York, 2002), pp. 1160–1164.
8. H. Schmidt, Y. Dongliang, and A. Hawkins, in *Integrated Photonics Research*, Postconference Digest, Vol. 92 of OSA Trends in Optics and Photonics Series (Optical Society of America, Washington, D.C., 2003), paper ItuC2-1.
9. R. F. Cregan, B. J. Mangan, J. C. Knight, T. A. Birks, P. St. J. Russell, P. J. Roberts, and D. C. Allan, *Science* **285**, 1537 (1999).
10. H. A. Jamid, *Appl. Opt.* **41**, 1385 (2002).
11. S. G. Johnson, M. Ibanescu, M. Skorobogatiy, O. Weisberg, T. D. Engeness, M. Soljacic, S. A. Jacobs, J. D. Joannopoulos, and Y. Fink, *Opt. Express* **9**, 748 (2001), <http://www.opticsexpress.org>.
12. C. L. Xu, W. P. Huang, M. S. Stern, and S. K. Chaudhuri, *IEE Proc. Optoelectron.* **141**, 281 (1994).